Ecological Monographs, 89(2), 2019, e01360

Multiple mechanisms confer stability to isolated populations of a rare endemic plant

Reilly R. Dibner,[1,4] Megan L. Peterson,[2] Allison M. Louthan,[3] and Daniel F. Doak[2]

[1]*Program in Ecology and Haub School of Environment and Natural Resources, University of Wyoming, Bim Kendall House, 804 E. Fremont Street, Laramie, Wyoming 82070 USA*
[2]*Environmental Studies Program, University of Colorado, Boulder, Colorado 80309 USA*
[3]*Department of Biology, Duke University, Durham, North Carolina 27708 USA*

Citation: R. R. Dibner, M. L. Peterson, A. M. Louthan, and D. F. Doak. 2019. Multiple mechanisms confer stability to isolated populations of a rare endemic plant. Ecological Monographs 89(2):e01360. 10.1002/ecm.1360

Abstract. The persistence of small populations remains a puzzle for ecology and conservation. Especially interesting is how naturally small, isolated populations are able to persist in the face of multiple environmental forces that create fluctuating conditions and should, theory predicts, lead to high probabilities of extirpation. We used a combination of long-term census data and a five-year demographic study of a naturally rare, endemic plant, *Yermo xanthocephalus*, to evaluate the importance of several possible mechanisms for small population persistence: negative density dependence, vital rate buffering, demographic compensation, asynchrony in dynamics among sub-populations, and source–sink dynamics. These non-exclusive explanations for population persistence all have been shown to operate in some systems, but have rarely if ever been simultaneously examined for the same population or species. We hypothesized that asynchrony in dynamics and demographic compensation would be more powerful than the other three mechanisms. We found partial support for our hypothesis: density dependence, asynchrony among population segments, and source–sink patterns appear to be the most important mechanisms maintaining population viability in this species. Importantly, these processes all appear to operate strongly at very fine spatial scales for *Yermo*, allowing the only two, extremely small, populations to persist. We also found considerable differences in the results of our census and demographic analyses. In general, we estimated substantially greater chances of population survival from the census data than from the shorter-term demographic studies. In part, this difference is due to drier than average climate conditions during the years of the demographic work. These results emphasize that while demographic information is necessary to understand various components of population dynamics, longer term studies, even if much less detailed, can be more powerful in uncovering some mechanisms that may be critical in stabilizing population numbers, especially in variable environments.

Key words: asynchrony; conservation biology; demographic buffering; density dependence; population viability; portfolio effect; rare species; source–sink dynamics.

Introduction

Small populations are particularly susceptible to extirpation (Honnay and Jacquemyn 2007) and the consequences of local extirpation are greatest for rare endemic species, for which local losses can be equivalent to global extinction (e.g., Maschinski et al. 2006, Dirnböck et al. 2011). Given these threats, a fundamental puzzle of ecology and conservation is how small populations, especially of globally rare species, manage to persist (Gaston and Kunin 1997). Rare species contribute substantially to biodiversity (Fisher et al. 1943, Preston 1948) but often have small and/or few populations (Rabinowitz 1981, Rabinowitz et al. 1986). Therefore, understanding the mechanisms that increase the chances of persistence is important to conserving global biodiversity. Additionally, anthropogenic impacts such as climate change have reduced many once abundant, wide-ranging species into a series of small, isolated populations, making an understanding of how small populations persist relevant for a wide range of taxa. Furthermore, the ability of species to migrate into newly suitable areas as climate shifts depends on the establishment and persistence of initially small and isolated populations.

A major force contributing to extinction risk is environmental stochasticity, which can differentially threaten small populations (Dennis et al. 1991, Boyce et al. 2006). In order to persist, populations must be resilient to natural levels of environmental variation, including climatic variability and disturbance. In small populations that are also too isolated for meaningful

Manuscript received 21 February 2018; revised 19 October 2018; accepted 24 October 2018. Corresponding Editor: Bruce G. Marcot.
[4] E-mail: reillydibner@gmail.com

inter-population movements, five non-exclusive mechanisms may confer this resilience: (1) negative density dependence can enable populations to recover from low densities due to high population growth rates when at low densities (Ginzburg et al. 1990, Sinclair and Pech 1996, Yenni et al. 2012); (2) different demographic rates can show opposing responses to the same environmental factors, an effect termed demographic compensation, so that population growth rate is buffered across a range of environmental conditions (Doak and Morris 2010, Villellas et al. 2015); (3) vital rate buffering, where variability of vital rates is negatively correlated with their importance for population growth, can reduce variability in population growth over time (Pfister 1998, Morris and Doak 2004, Rotella et al. 2011, but see Jongejans et al. 2010, Jakalaniemi et al. 2013, Bjørkvoll et al. 2016, McDonald et al. 2016); (4) asynchronous responses to environmental fluctuations among subpopulations or individuals can stabilize numbers and thus buffer populations from extinction via the portfolio effect (e.g., Moore et al. 2010, Schindler et al. 2010, Abbott et al. 2017), as they do for community characteristics (Doak et al. 1998, Hilborn et al. 2003); and (5) fine-scale source–sink dynamics, wherein parts of a population with consistently high growth rates (sources), can subsidize lower quality parts of a population (sinks) through dispersal (Pulliam 1988, Doak 1995, Dias 1996, Kauffman et al. 2004).

Despite evidence that these mechanisms can theoretically stabilize population numbers and buffer small populations against extinction (Fiedler 1987, Barot and Gignoux 2004, Lloret et al. 2012), few studies have tested for the presence or importance of each of these effects in the same system. Here, we test the extent to which the mechanisms described above (negative density dependence, vital rate buffering, demographic compensation, asynchrony in dynamics among sub-populations, and source–sink dynamics) contribute to persistence of a rare endemic plant, Desert Yellowhead (*Yermo xanthocephalus* [Asteraceae], hereafter *Yermo*). We hypothesized that two of these mechanisms, asynchrony in dynamics and demographic compensation, would be far more powerful than the other three because *Yermo* populations are sparse, spatially stable, and temporally unstable (all documented by Scott and Scott 2009). In addition, we hypothesized that responses to precipitation variability would be the primary driver of fluctuating vital rates and population growth, with spatial variation in these responses accounting for the majority of any portfolio effects.

To evaluate the presence and importance of these mechanisms, we combined long-term (>10 yr) census data (which we used to test for asynchrony and density dependence in sub-population abundance and growth rates, and source–sink dynamics), with detailed shorter term (three to four annual transitions) demographic data (which we used to test for vital rate buffering, demographic compensation, and patterns of source–sink dynamics). We also evaluated population viability using both of these data sets, providing a rare comparison of predictions of the two most common types of population viability analyses (PVA) data sets: annual abundance estimates and demographic data.

Methods

Study species

Yermo is a rare, perennial herb occurring in a monospecific genus that is endemic to central Wyoming (Appendix S1: Fig. S1), USA. Since its discovery in 1990, *Yermo* has attracted attention for its unusual geographic distribution, taxonomic uniqueness, and extreme rarity. In 2002, the species was listed as threatened under the USA Endangered Species Act, and remains so currently (50 CFR §17.96, USDI 2002). *Yermo* is known to occur in only two populations in central Wyoming that together total fewer than 22 inhabited hectares. Approximately 17 occupied hectares are at the Sand Draw location (Scott and Scott 2009), and five are at the more recently discovered Cedar Rim site (Appendix S1: Fig. S1; Heidel et al. 2011). In both populations, *Yermo* occurs in shallow limestone and sandstone Entisols on steep slopes and sandy hollows with wind-blown deflation; both of these types of habitat have much lower plant cover than the surrounding sagebrush-dominated shrublands (Heidel et al. 2011).

Although distinctive in appearance (Appendix S1: Fig. S2), the species is a relatively typical perennial forb in its life history. Individuals have spatially limited clonal growth, so that physiological isolated units are thought to be fairly easily distinguished from one another by distance (Scott and Scott 2009). New plants establish from seed, grow for a minimum of five years before flowering, and often have non-reproductive years after their first flowering event (Scott and Scott 2009). No direct data on seed dormancy exist for the species, although the highly erosive habitat and relatively large seed size make a substantial seed bank unlikely.

Census data and analyses

Scott and Scott (2009) collected complete census data of all *Yermo* plants in the Sand Draw population from 1995 to 2004, with only one year of missing data (1999). To conduct accurate, spatially structured censuses, they delineated 1-ha squares with permanent stakes and censused each 10 × 10 m subsection in each 1-ha square. The resulting 10 × 10 m squares (hereafter 100-m^2 plots; Appendix S1: Fig. S1, Table S1) formed a grid that covered the entire area occupied by *Yermo* at Sand Draw, the only known population of the species at the time. In July 2013, we re-censused this grid following the Scotts' exact methodology. We used this long-term census data to test for three of the mechanisms that could contribute to resiliency in this population: density

dependence, asynchrony among subpopulations, and source–sink dynamics.

Population growth.—We first estimated annual population growth rates within each 100-m^2 plot and also for the entire Sand Draw population. We estimated annual growth rates as $\lambda_t = (N_{t+i}/N_t)^{1/i}$, where i is the number of years between observations, N is population size, and t is time (years). We excluded the 2004–2013 transition from most analyses due to the large gap in sampling, failure to meet assumptions of approaches accounting for sampling gaps (e.g., Dennis et al. 1991; Appendix S1: Fig. S3), and because of our interest in tying λ_t to annual climate drivers. The spatial distribution of *Yermo*, including plot-specific densities, was fairly constant across the years of the study, and many of the 384 100-m^2 plots that supported *Yermo* plants had low mean densities of fewer than 30 individuals. To accommodate zeros in the data set, we added 1 to all counts prior to calculating λ_t, but also excluded transitions with true starting abundances of 0, as these years do not provide meaningful information on population growth rates. For our analyses of plot-level population dynamics, we excluded plots with fewer than five yearly transitions, leaving 326 plots representing >99% of the population. However, given the consistently low densities, high demographic stochasticity, and missing data in many of these plots (see Appendix S1), we also repeated analyses using only plots with data for all eight yearly transitions and a mean abundance of at least 30 individuals. This approach focused on 114 plots that, together, represented 82% of the population.

To assess synchrony among populations occurring in different patches, we examined pairwise Pearson correlations in $\log(\lambda_t)$ among plots. We tested for relationships between different metrics of plot quality, including mean abundance ($\bar{N}$), mean growth rate, $\overline{\log(\lambda_t)}$, and the mean correlation coefficient in $\log(\lambda_t)$ of a plot with all other plots weighted by each plot's mean abundance (hereafter $\bar{\rho}$).

Source–sink dynamics.—Results from the analyses described above also indicate whether or not there are consistent spatial differences in average population performance, a necessary pre-condition for source–sink dynamics. While we did not have data on movement of seeds between transects, we could still identify whether fine-scale differences in growth rates were present; such a pattern could indicate habitat quality effects that would allow source–sink patterns within the population.

Density dependence.—To quantify population growth patterns, we fit both density-dependent and density-independent models to the census data. We tested for density dependence across the entire Sand Draw population as well as within individual plots. We modeled *Yermo* abundance at time $t + 1$ as a negative binomial mixed model (glmm) with an offset for $\log(N_t)$, following the general approach of Abbott et al. (2017) and Brown and Crone (2016). We compared Ricker models, which include a fixed effect of abundance at time t (Ricker 1954), to density-independent models. For analyses at the plot level, we compared models with random intercepts and/or slopes among years and/or plots with the Akaike information criterion, corrected for sample size (AIC_c). We fit all models with the lme4 package (Bates et al. 2015) in R 3.2.3 (R Core Team 2016). The best supported model was a Ricker model including random variation in the intercept among years and random variation in the intercept and slope among plots.

Asynchrony among subpopulations.—We used three analyses to test for asynchrony in population growth among 100-m^2 plots and to identify how differences in plot-level responses to environmental drivers could account for any asynchrony in the Sand Draw population. To identify if the magnitude of correlations between plots in log (λ_t) or log N was related to their spatial distance from one another, we used Mantel tests. Since the north-south axis most closely corresponds to the slope and hence microhabitat at Sand Draw (higher elevation in the north, lower in the south), we considered Euclidean distance along this axis as well as two-dimensional distance and distance on the east-west axis.

We then quantified the strength of asynchrony among plots and its contribution to population stability with two commonly used empirical metrics: the population-level synchrony index (Loreau and de Mazancourt 2008, Thibaut and Connolly 2013), and the mean-variance portfolio effect (PE; Anderson et al. 2013). The population-level synchrony index ranges from zero (if all plots are perfectly asynchronous or abundance is constant) to one (if all plots are perfectly synchronous) and a PE greater than one indicates stabilizing effects of among-plot variance on total population size (see Supporting Information for details).

We also tested for climatic drivers of population growth and asynchrony in plot-level responses to climate variation. We downloaded climate data from the nearby Riverton, Wyoming NOAA station (Appendix S1: Fig. S4) and summarized the climate data into annual (July–June before census) and spring (April–June before census) precipitation sums and temperature means; these variables are likely important for *Yermo* performance and correspond with the timing of our demographic surveys in late June to mid-July (data *available online*).[5] We tested whether each of these climate variables explained variation in $\log(\lambda_t)$ among years by comparing negative binomial glmm Ricker models of population growth, as described above, that included one of the four climate variables with AIC_c. In particular, we compared Ricker models with random variation in intercepts and slopes among plots, but that substituted fixed effects of climate in each year for randomly varying intercepts in each

[5] wrcc.dri.edu/WRCCWrappers.py?sodxtrmts+487760+por+por+pcpn+none+msum+5+01+F

year. For each climate variable, we fit models that considered linear and quadratic effects of climate and their interactions with plot position along the north-south axis, capturing interactions between climate and the main spatial variation in habitat. Although models with random year effects had the lowest AIC_c, the best-supported model with climate variables had similar explanatory power, especially when excluding sparse plots with high demographic stochasticity (see *Results*). We therefore used the best-supported climate model; this model included linear and quadratic terms for annual precipitation and an interaction between North-South plot position and annual precipitation, allowing for inferences about how annual climate shapes population dynamics. While multiple climate factors are likely to drive *Yermo* dynamics, our data were too temporally limited to fit multifactor models.

Simulations.—To estimate the future viability of the Sand Draw population, we constructed a multi-site count-based PVA based on analyses of the long-term census data (Morris and Doak 2002). These models can incorporate correlated responses among plots and negative density dependence into population predictions, but do not include dispersal as we have no data on seed movement within the Sand Draw population. To predict future population numbers, we simulated population growth in each time step by estimating an expected log (λ_t) for each plot based on its abundance, climate variable, and the plot-specific coefficients from the best-supported Ricker model. To this expected log(λ_t) value, we added a plot-specific correlated random value estimated from the covariance matrix of the model residuals among plots (following Abbott et al. 2017); this addition allows inclusion of unexplained covariance among plots after accounting for density and climatic effects.

We tested the ability of these simulations to capture *Yermo* population dynamics by using observed plot abundances at the start of the census in 1995 as starting values and simulating dynamics based on the observed sequence of precipitation from 1995 to 2013. These simulations showed good concordance with observed dynamics (correlation coefficient = 0.73 and 0.80 for log (λ_t) and total abundance, respectively). We next simulated long-term viability of the population by using abundances in 2013 as starting numbers and randomly drawing annual precipitation values from a normal distribution with mean and variance taken from the 99 complete observations of annual precipitation from the Riverton NOAA station between 1908 and 2015 (Appendix S1: Fig. S4). We replicated all simulations 10,000 times over a 100-yr time window. Because the probability of quasi-extinction (i.e., <100 individuals) is very low, we estimated the probability that the total abundance across all plots would decline below a range of threshold population sizes, expressed as a proportion of the observed minimum population size, within 10, 50, and 100 yr into the future.

We ran two additional population simulations to estimate the stabilizing effects of density dependence and spatial asynchrony, particularly in climate responses, to long-term viability. First, we ran simulations that were based on an alternative model that removed effects of spatial asynchrony in climate responses (see Supporting Information for details). Second, we ran simulations based on models that removed stabilizing effects of density dependence, while still imposing a density cap on numbers. Finally, we ran simulations that removed both simultaneously (see Supporting Information for details).

Demographic data and analyses

To test the strength of vital rate buffering, demographic compensation, and patterns of source–sink dynamics as potential mechanisms of population stability, we conducted detailed demographic surveys of *Yermo* in both populations. We conducted these surveys from 2010 to either 2014 for the Sand Draw population or 2013 for Cedar Rim, giving three to four annual transitions of demographic data. In 2010, we established 11 permanent sampling transects within the census grid at the larger Sand Draw population and five at Cedar Rim (Appendix S1: Fig. S1, Table S2). At both sites, we established transects that span the range of habitat types occupied by *Yermo*, from steep upper slopes to relatively flat lower areas. We exhaustively searched each transect from late June to mid-July to find and map new seedlings or previously unmarked plants and to re-locate existing plants. To be consistent with the previous census work on *Yermo* (Scott and Scott 2009), we designated plants as separate individuals if the base of the rosettes were more than three centimeters apart; in instances where basal rosettes of the same individual were occasionally farther apart in one or several years, we were careful to match these plants with previous data records. For each plant, we measured the total number of basal leaves, the length of the longest leaf, the number of inflorescences, and the number of flowering heads per inflorescence. We summarized size as the natural log of the product of the single longest leaf and the total number of leaves. We used the total number of flowering heads as our measure of potential reproductive output.

Vital rate estimation.—We characterized the demography of *Yermo* using continuous, size-dependent functions for each main vital rate: growth, variance in growth, survival, probability of flowering, and number of flower heads if flowering (Easterling et al. 2000, Morris and Doak 2002). We also estimated several other demographic rates: seedling survival over the first year of life, seedlings per flower head in the previous year, the number of new plants arising from vegetative reproduction (new non-seedling plants) appearing each year, and size distributions for surviving seedlings and new non-seedling plants. For each of the main vital rates, we fit a series of alternative general linear models (GLMs), and

used AIC_c comparisons to identify the best-supported model (cf., Doak and Morris 2010, Palmer et al. 2010, Raventós et al. 2015). These alternative models included effects of size, size squared, year (categorical), population, transect, and all possible two-way interactions between these terms. We conducted preliminary analyses to see if combining transects into only five groups would be supported, but found that model selection criteria strongly favored use of the 16 transects originally identified. We also tested for effects of density dependence or annual precipitation on each vital rate but found no support for these effects (e.g., AIC_c values for survival and mean growth increased by 98–186 if precipitation was substituted for a categorical year effect or density was substituted for a transect effect), which is unsurprising given only four annual transitions of data. We used logistic models for survival and probability of flowering, while all other vital rates were modeled assuming normally distributed errors.

We used transect-level analyses to estimate some vital rates that could not be linked to individuals. In particular, we used summed plant size on transects to fit models of the number of new plants arising from vegetative reproduction per existing plant per year, and we used the total number of flower heads produced per transect per year to estimate seedlings arising per flower head. Seedling survival and the size distributions of seedlings and new plants were not fit to alternative models, as the sample sizes were too low for meaningful model comparisons.

Population growth and viability.—We constructed separate annual projection models for each of the 16 transects and over each annual transition (four at Sand Draw and three at Cedar Rim). We used the best-supported model for each vital rate to determine continuous size-based transition kernels, resulting in an Integral Projection Model (Easterling et al. 2000, Ellner and Rees 2006) for each transition and transect. We estimated the kernel for all transitions not ending in seedlings as $N(y) = \int s(x)g(x,y) + m(x,y) + r(x,y)$, where $s(x)$ is the probability of survival as a function of initial size x, $g(x,y)$ is the probability of growing or shrinking from initial size x to size y at time step 2, $m(x,y)$ is the expected number of new, non-seedling plants of size y produced per plant of size x, and $r(x,y)$ is the probability of seedlings transitioning to size y a year later, which is equal to the product of S_{sdling}, the one year survival of a seedling, and $g(y)$, the probability that a surviving seedling will be size y in its second year. For transitions ending in seedlings, the kernel is the integral of the product of pr(x), the probability of reproduction of an individual of size x, $f(x)$ the expected number of flowering heads if reproducing, and flrseedling, the number of seedlings expected to be seen in a year later per flowering head. We used the kernel for each transition and transect to make a matrix based on 90 evenly spaced mesh points, as well as a category for seedlings.

Based on the resulting matrices, we estimated annual transect-specific λ values and compared these predictions to observed annual λ based on simple counts of individuals within each transect in each year. We also computed the distributions of 100-yr stochastic growth rates (λ_S) for each transect, starting each simulation at the stable size distribution of the mean matrix of each transect by a matrix randomly sampled from among the three to four annual matrices for a given transect over 100 time steps and repeating this process 1,000 times. We accounted for estimation uncertainty in all kernels used in this simulation by sampling from the uncertainty in all vital rate parameter estimates when constructing kernels and hence matrices (Bakker et al. 2009). We did not include vital rate model uncertainty in these estimates, given high support for the top model for all vital rates with high elasticity values (Appendix S1: Table S3). We compared distributions of λ_S based on simulations with equal sampling of years with simulations in which the two driest years had only a summed 16% chance of being chosen in each time-step, as years this dry have only occurred 16% of the time in the previous century according to the Riverton NOAA climate data (see footnote 5).

To estimate extinction risk for each transect we used the same simulation approach. We did not have a good estimate for the fraction of the population represented demographically by each transect, so we started the simulations for each transect with 500 plants. We asked if, using 500 simulations of 100 yr each, the population declined to 10% of the starting numbers; if this decline occurred, we asked how long it took to reach this threshold. These simulations were conducted incorporating estimation uncertainty with vs. without weighted sampling of dry years, as described above. Furthermore, we added a population cap equal to 1.25 times the starting number to enforce realistic limits to population size.

Source–sink dynamics.—The analyses just described give estimates of consistent spatial differences in λ_S, which are a precondition for source–sink dynamics. As for our analyses of census data, we had no movement estimates so could only test for differences in λ, rather than parameterizing models to estimate source–sink dynamics directly.

Vital rate buffering.—To test whether the vital rates to which *Yermo* population growth is most sensitive are fairly consistent over time, we used the general approach of Pfister (1998) and Morris and Doak (2004), comparing the variability of vital rates to their elasticity values. We characterized variability by the coefficient of variation (CV) for the mean and variance of growth and flower number, which have undefined upper bounds, or by relative CV, the CV scaled by its maximal possible value given its mean, for [0,1] vital rates, including survival and reproduction probabilities (Morris and Doak 2004). We used the standard perturbation approach

(Caswell 2001, Morris and Doak 2002) to estimate elasticity values for nine groups of 10 size classes each, and represented the CV of each size group's vital rate by calculating the CV of the median size's vital rate. We summarized the results of these analyses of temporal relationships separately for each vital rate type and for all vital rate estimates. While similar studies have generally focused only on temporal variation, we also looked for evidence for lowered spatial variance in vital rates, repeating the above analysis for year-specific spatial CV in mean vital rates for each transect. We also use these results to simulate stochastic population growth with vs. without variance-elasticity correlations of vital rates, described in Demographic compensation.

Demographic compensation.—To test for patterns indicative of demographic compensation, we used correlations between the coefficients for year effects in each of the vital rate functions that showed temporal variation: survival, mean growth, variance in growth, probability of reproduction, and flower to seedling survival. For mean and variance of growth, which have year × transect interactions, we used interaction coefficients to generate an average spatial or temporal effect. Negative correlations in year coefficients of different vital rates indicate demographic compensation. Since these coefficients were already supported by model selection for each vital rate, and since the sample sizes for annual variation were very small, we did not assess significance of these relationships using randomization procedures (cf., Villellas et al. 2015). We also performed parallel analyses using transect coefficients for spatially varying vital rates to look for evidence of spatial demographic compensation. We used these results to simulate stochastic population growth with vs. without demographic compensation, described in Effects of vital rate buffering and demographic compensation on population growth.

Effects of vital rate buffering and demographic compensation on population growth.—We tested the importance of temporal variance-elasticity patterns or demographic compensation for population growth using randomization procedures to simulate 500 stochastic growth trajectories over 100 yr without one or both of these patterns (see Supporting Information for details of simulation procedures). We conducted these simulations separately for each transect, and compared the results with point estimates of transect-specific long-term stochastic growth rates. We also performed simulations with manipulations of variance-elasticity or demographic compensation for only one vital rate type at a time.

Results

We found variable support for the five stabilizing mechanisms we tested: density dependence, asynchrony among subpopulations, vital rate buffering, demographic compensation, and source–sink dynamics. Due to differences in the methodologies used to analyze the census vs. demographic data, we present results from these sets of analyses separately.

Census data

Population growth and source–sink dynamics.—The Sand Draw population varied between 9,224 and 13,063 total plants seen during the years of study, showing fairly high stability. We also found a high correlation between the average number of plants found by Scott and Scott (2009) in each 100-m^2 plot from 1995 to 2004 and the number we found in 2013 (Pearson's $r = 0.82$), showing stability in the dispersion of the population. We found *Yermo* in only a single 100-m^2 plot where Scott and Scott (2009) had never found the species. Population numbers within plots fluctuated considerably and not all parts of the population were synchronized in their fluctuations (Fig. 1). Plots had mean λ_S values ranging from 0.837 to 1.218, showing support for possible source–sink dynamics. Overall, the entire Sand Draw population had a mean λ_S of 1.027 and 1.034 (including or excluding the 2004–2013 transition, respectively). Estimates of mean λ_S were lower using the Dennis et al. (1991) regression method, because the longer transition (2004–2013) was an outlier.

Density dependence.—We found negative density dependence in population growth rates, both for individual plots and for the entire Sand Draw population (Appendix S1: Fig. S5). AIC_c indicated a Ricker model as a better fit to population growth rates compared to density-independent models for both the entire Sand Draw population ($\Delta AIC_c = 8.64$) and for individual plots ($\Delta AIC_c > 4.00$; Appendix S1: Table S4). For plot-level analyses, AIC_c supported randomly varying intercepts and slopes among plots, suggesting plot-specific density effects (Appendix S1: Table S4). These results were robust to analyses excluding sparse plots (Appendix S1: Table S5). For individual plots, the slopes of $\log(\lambda)$ on starting abundance ranged from -0.037 to -0.001; the slope for the entire Sand Draw population was -1.17×10^{-4}.

Asynchrony among subpopulations.—The degree of synchrony depended on spatial scale, but we found substantial evidence of asynchrony across plots. Annual population growth rates were not well synchronized, with pairs of plots ranging from highly positively correlated to weakly or negatively correlated (Fig. 1). Further, both abundance and λ_t were strongly correlated through space, with plots closer together having more similar values (Appendix S1: Figs. S6 and S7). Not surprisingly, the majority of this effect comes from north-south distance as these distances span the elevational gradient at the site, and thus are likely to correspond to sharp differences in habitat (Appendix S1: Fig. S7). While these effects are strong at short distances, they fall off at two-dimensional distances over about 150 m (Appendix S1:

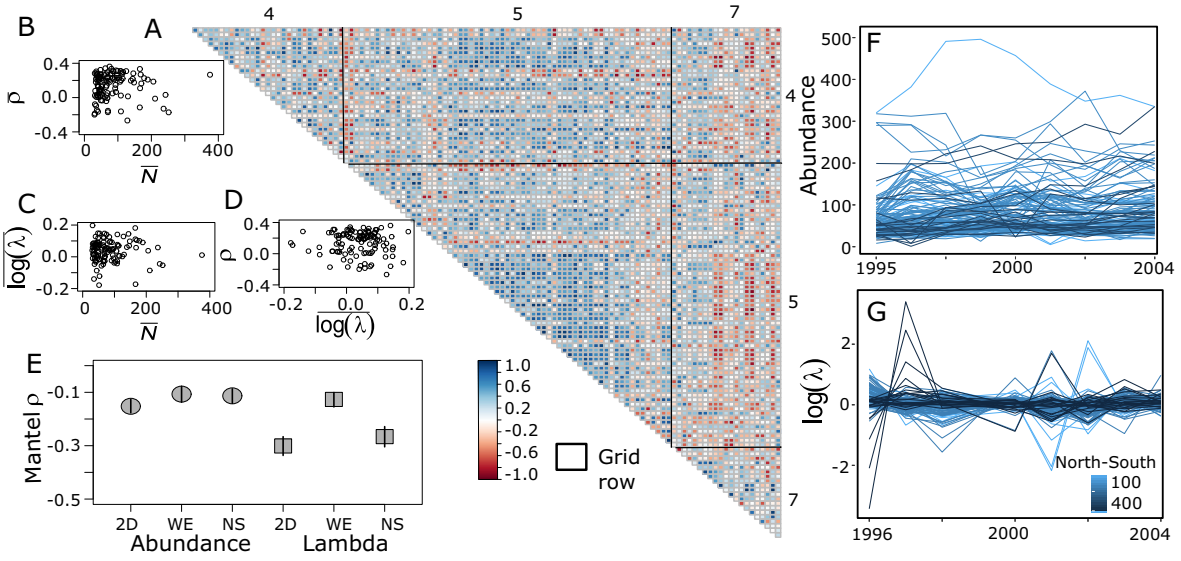

FIG. 1. (A) Correlation matrix in log(λ) between plots from 1995 to 2004; solid lines delineate rows in the census grid (see Appendix S1: Fig. S1) and plots are ordered by their west-east position within north-South rows. (B–D) Relationships between plot-level metrics including the mean correlation coefficient $\bar{\rho}$, the mean population growth rate $\overline{\log(\lambda)}$, and the mean abundance $\bar{N}$ within each plot. (E) Mantel test statistics and 95% confidence intervals for correlations in log abundance or log(λ) with distance in two dimensions (2D) or along a west-east (WE) or north-south (NS) dimension. The north-south dimension most closely corresponds to the slope at Sand Draw (higher elevation in the north, lower in the south) and thus microhabitat differences for *Yermo*. Correlation coefficients decrease with increasing distance, especially in log(λ) along the north-south dimension. (F) Abundance and (G) log(λ) of 100-m^2 plots based on census counts from 1995 to 2004 (2013 not shown). Shading is proportional to position along the north (lighter blue) to south (darker blue) axis of the census grid. Note asynchrony in *Yermo* abundance and log(λ).

Fig. S7), much less than the spatial scale of the entire population. This spatial asynchrony strongly reduced variability in growth rate of the Sand Draw population as a whole; the synchrony index (ϕ) was 0.124, where zero indicates perfect asynchrony and one indicates perfect synchrony, and the portfolio effect (PE) was 2.18, where values greater than one indicate stabilizing effects of among-plot variance on total population size (Appendix S1: Fig. S8).

Finally, while annual precipitation explained variation in growth rates among years, there was AIC_c support for an interaction between precipitation effects and the position of plots along the north-south axis. Both linear and quadratic terms for precipitation variables were present in the best-supported climate model (Appendix S1: Tables S6–S7), indicating that population performance declined in particularly wet or dry years. However, wetter years had stronger negative impacts in more northerly plots, which are at higher elevation, whereas drier years had stronger negative impacts in more southern plots (Appendix S1: Fig. S9).

Effects of synchrony and density dependence on risk of population decline.—Our simulation models indicated a very low risk of catastrophic decline for this population. In our main simulations, the risk of the population declining to the observed minimum abundance was 28% over 100 years, but decline to below 80% of the observed minimum abundance was less than 0.2% (Fig. 2A). However, simulations incorporating sparse plots underestimated the risk of decline, showing less than a 15% chance of reaching the minimum population size observed in the census data over 100 yr. This discrepancy is likely due to the obscuring effects of demographic stochasticity; models parameterized with all plots did a poorer job of predicting the dynamics of the 114 plots containing most individuals relative to models fit excluding sparse plots (correlations between model predictions and data were 0.338 and 0.674 for models with and without sparse plots, respectively). For this reason, we emphasize results from simulations excluding sparse plots, which accurately capture the observed population dynamics (correlation between simulated and observed population abundance from 1995 to 2013 = 0.80).

Spatial asynchrony among plots and the stabilizing effects of negative density dependence both contributed strongly to population stability (Fig. 2B). Simulations removing the effects of spatial asynchrony or negative density dependence increased the probability that the population would decline below 80% of the observed minimum abundance within 100 yr to 56% and 7%, respectively, while simulations removing both stabilizing effects increased this probability to 97%.

Demographic data

We recorded data on 1,697 individuals in our study transects, for a total of 6,923 plant-years of data across

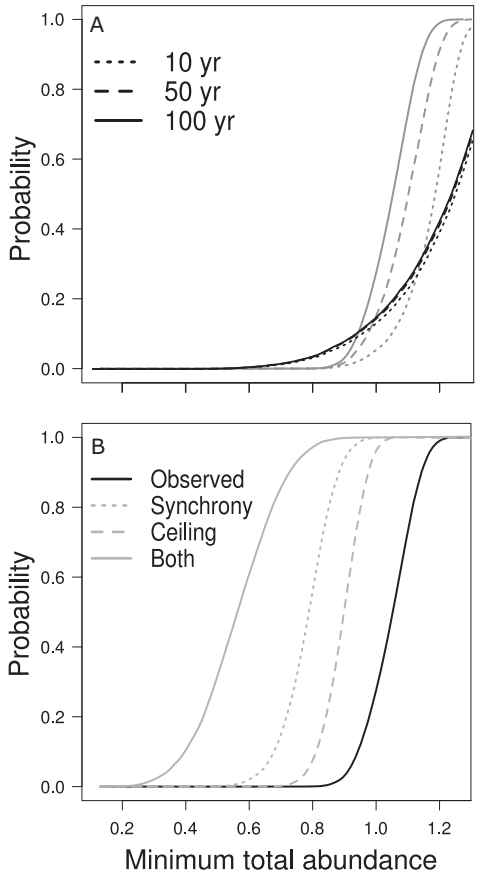

FIG. 2. (A) Multi-site count-based simulations of *Yermo* population dynamics suggest little risk of substantial declines in abundance within 10 (dotted), 50 (dashed), or 100 (solid) years in viability simulations based on the best-supported Ricker model fit to all plots (black lines) or excluding sparse plots (gray lines). Simulations include plot-specific precipitation responses and drawing annual precipitation values with the observed mean and variance from the last century. (B) Different stabilizing mechanisms contribute to this overall stability (black line), as shown by increased risk of decline in simulations removing all asynchrony among plots (gray dotted), removing the stabilizing effects of density dependence (gray dashed), and removing all stabilizing mechanisms (gray solid). The *x*-axis gives the minimum total abundance expressed as a proportion of the minimum abundance observed from 1995 to 2013, 9224 individuals.

the four annual transitions studied. We found strong support for year and transect effects on most vital rates (Appendix S1: Table S3, with model results). Survival rates were strongly size dependent, peaking at roughly 0.70 to 0.95 for intermediate-sized plants, with considerable variation across years and transects (Appendix S1: Table S3, Fig. S10). Growth rates were also size dependent, with shrinkage and growth of individual plants common, and varied with year, transect, and an interaction between year and transect (Appendix S1: Table S3, Fig. S11). We found year and transect effects on probability of reproduction, while the number of flowering heads given reproduction varied with plant size and year, but not transect (Appendix S1: Table S3, Figs. S12 and S13). The best supported model for number of seedlings per prior year's flower heads included year effects (2013–2014 had by far the highest seedling establishment rates; Appendix S1: Fig. S14), but we cannot infer differences across transects because we used summed data for each transect. Finally, the number of newly found non-seedling plants was predicted to vary with the summed sizes of existing plants, but not year or location (Appendix S1: Table S3, Fig. S15). Effects of existing plant sizes on this vital rate are consistent with these new plants being either individuals that were dormant in a year, or new ramets that are asexual daughters of existing plants.

Predicted population growth and source–sink patterns.—Different years and transects showed very different predicted annual growth rates, with values ranging from 0.473 to 1.097. Stochastic growth rates were similarly variable across transects, and indicated that some parts of the population had substantially higher growth rates than others. In models that used weighting of dry years, two transects had distributions of λ_S that are largely greater than one, four others straddle one, and several others have distributions entirely greater than 0.90–0.95 (Fig. 3A), while other transects are predicted to have substantial declines. Unweighted models were largely similar though somewhat more pessimistic (Appendix S1: Fig. S16). We found reasonably good correspondence between IPM-estimated λ_t and observed count-based lambdas from the demographic transects (Appendix S1: Fig. S17, Spearman rank correlation = 0.56), with the demographic models generally predicting a narrower and slightly lower range of growth rates compared to those seen from the longer census study (Appendix S1: Fig. S18). However, growth rates estimated from the census and demographic studies showed little spatial correspondence, suggesting that the observed differences may not correspond to stable differences on mean growth (Appendix S1: Fig. S19).

Populations in all transects were predicted to have moderate to high probabilities of falling below a 10% threshold over 100 yr, when accounting for parameter uncertainty as well as environmental stochasticity. However, this risk was fairly low for some transects, which were also predicted to persist for at least 40 yr before reaching the threshold (Fig. 3B). These patterns were similar if not weighting the prevalence of dry years (Appendix S1: Fig. S16) but were strikingly less optimistic than the predictions of the density-dependent models based on the long-term census data (Fig. 2).

Vital rate buffering.—Elasticity values, the proportional effect of changes in different vital rates on population growth, generally conformed to expected patterns for a species with moderate lifespan (Fig. 4). Elasticities were highest for survival and mean growth rates, which together determine the chances of a plant surviving and

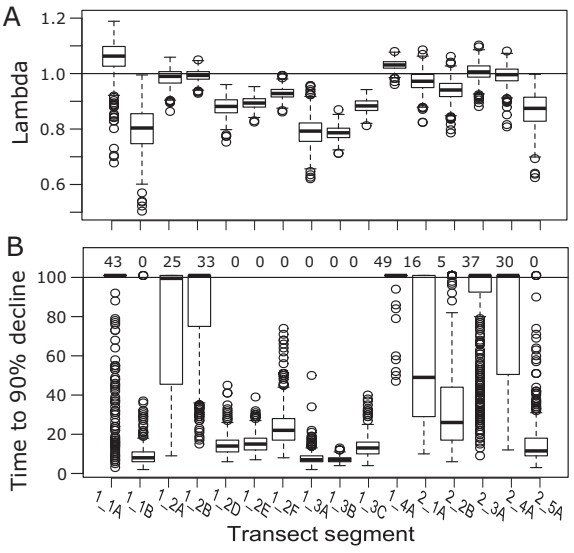

FIG. 3. Population growth and decline risk based on demographic projections. (A) Distributions of stochastic lambda estimates for different transects, weighting by observed frequencies of dry years. Distributions come from 500 simulations of 100 yr of future growth. Models are based on draws from the observed annual population matrices that account for the frequency of dry vs. normal or wetter years, and also account for parameter estimation uncertainty. (B) Probabilities of decline to 10% of starting numbers in simulations run separately for each transect and including unequal weighting of years to reflect the probability of dry vs. normal precipitation. These simulations included a population cap at 1.25% of starting numbers and parameter uncertainty. Box plots show the distribution of time to reach this population threshold for 500 replicate simulations. Tukey box plot components are mid line, median; box edges, upper and lower quartiles; whiskers, extend to the upper and lower fences at 1.5 times the interquartile range; and points, outliers beyond fences. Points above 100 yr indicate that a simulated population never reached the threshold. Numbers above the line at 100 yr are the probability of never reaching the 100% threshold.

growing to sizes that have substantial reproductive success. In addition, elasticity values for these two vital rates peaked at intermediate sizes, showing a balance of greater importance of larger, older plants, but also the reduced effects of changes in vital rates that only influence the fairly uncommon largest classes. We found mixed evidence for low temporal variability of the vital rates with the highest elasticity values. Across both binomial variables (probabilities of survival and reproduction) we saw a significant positive effect of elasticity on relative CV (linear regression coefficient = 0.308, $P < 0.0001$; Fig. 5A); however, for the survival rates (which have a higher elasticity and are thus more important for population growth), the relationship was significantly negative (coefficient = −0.175, $P < 0.001$). For non-binomial vital rates, we saw a highly significant negative relationship for temporal variation and elasticities across all vital rates (coefficient = −1.077, $P < 0.00001$, Fig. 5B) while, individually, there was a significant relationship for flowers, which was also negative (coefficient = −28.342, $P < 0.0001$).

Results for spatial variation and elasticities were similar, with significant positive and negative relationships for reproduction and survival respectively (reproduction coefficient = 44.333, $P < 0.0001$; survival coefficient = −0.237, $P = 0.0342$, Fig. 5C). For non-binomial vital rates, no single vital rate had a significant relationship between CV and elasticity, but across all vital rates the relationship was significant and negative (coefficient = −1.123, $P = 0.000424$, Fig. 5D).

Demographic compensation.—We saw evidence for negative correlations in time and space between different vital rates, indicative of demographic compensation (Table 1). In particular, we found substantial negative correlations among multiple vital rates through time. Most importantly, given their high elasticity values, mean growth and survival were strongly negatively correlated ($r = -0.83$) as were survival and reproductive probability ($r = -0.80$). Three other pairs of vital rates were also correlated with r between −0.78 and −0.97. With only four transitions of data to estimate temporal correlations, we could not draw strong conclusions from these results; however, they do indicate that vital rates almost certainly do not respond synchronously to environmental variation over time.

We found similar evidence of spatial demographic compensation across transects (Table 1). Three of the six correlations among transects were negative and the magnitude of negative and positive correlations was comparable. Survival and reproduction were strongly negatively correlated across space ($r = -0.50$), similar to the pattern across time, whereas growth and survival were essentially uncorrelated across space ($r = -0.07$).

Effects of vital rate variability and compensation patterns on population growth.—Eliminating either vital rate buffering or demographic compensation had substantial effects on stochastic growth rates for some but not all transects, with the overall effects of these mechanisms being quite weak. In addition, the consistency of these effects differed substantially across the two types of effect. In contrast to the assumed effects of vital rate buffering, removing observed CV–elasticity negative correlations resulted in generally higher λ_S in six transects, but lower growth in several more, and with little effect in others (Fig. 6). In contrast, removing demographic compensation substantially reduced λ_S in four transects, with little effect in the others. The net effects of removing both patterns were roughly additive.

We compared the relative effect of these perturbations with those for which we removed the observed demographic compensation or CV–elasticity mechanism for just one vital rate type at a time; this comparison revealed that some vital rates play a disproportionate role in generating the overall stabilizing effect (Fig. 6). In particular, probability of reproduction drives the vast majority of the stabilizing effect of removing CV–elasticity correlations in many transects, although one outlier transect, 1_3A, also

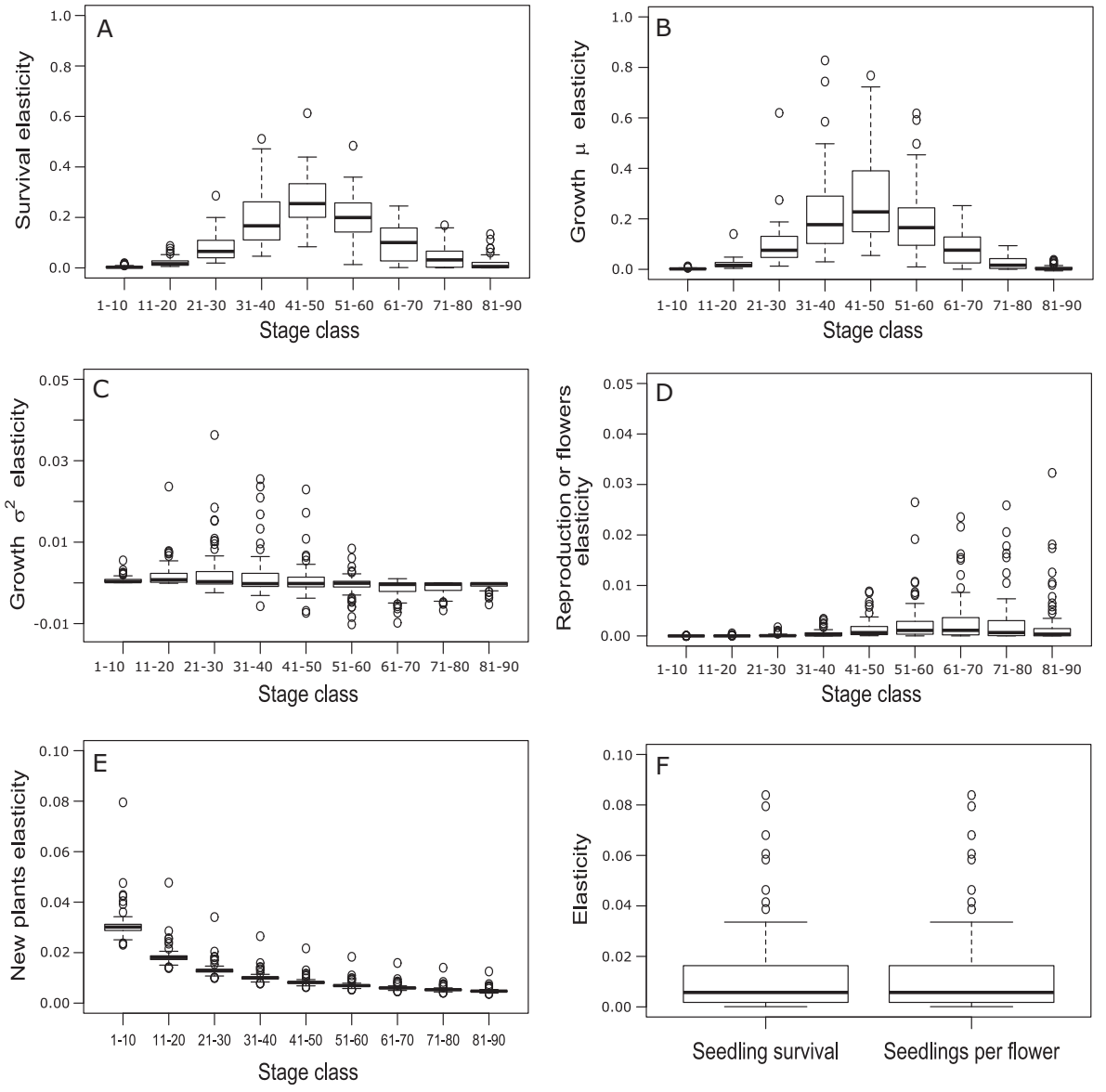

FIG. 4. Sensitivity of population growth to vital rates for *Yermo* to (A) survival (B) mean growth C) growth variance (D) probability of reproduction or number of flowers (E) probability of new plants (F) seedling survival and seedlings per flower. Elasticity values (proportional change in growth rate with a proportional change in a vital rates) are shown for each rate, with changes in rates made for sets of 10 of the 90 size classes used in the model construction at a time. Box plots show the range of elasticity values over each transect and annual model, which were analyzed separately. Box plot components are mid line, median; box edges, upper and lower quartiles; whiskers, extending to the upper and lower fences; and points, outliers beyond fences.

had strong effects of removal from two other vital rates (growth mean and variance). This effect is likely due to the strongly positive relationship between relative CV and elasticity for reproduction (Fig. 4A). Similarly, removing temporal correlations of flower number with other vital rates reproduced most of the overall demographic compensation effects (Fig. 6), a result that appears to come from negative correlations of flower number with all other time-varying vital rates besides survival (Table 1). These analyses also indicate that some destabilizing effects of individual rates types are masked when considering the net stabilizing effect of all vital rates. For example, removing the observed CV–elasticity relationship for survival alone resulted in considerable decreases in λ_S, showing that the observed relationship for survival actually destabilizes λ_S.

DISCUSSION

With a limited range and a total population size of fewer than 15,000 individuals, *Yermo* seems like a species that would be in dire risk of extinction. The high endemism of the species appears to be natural, however, rather

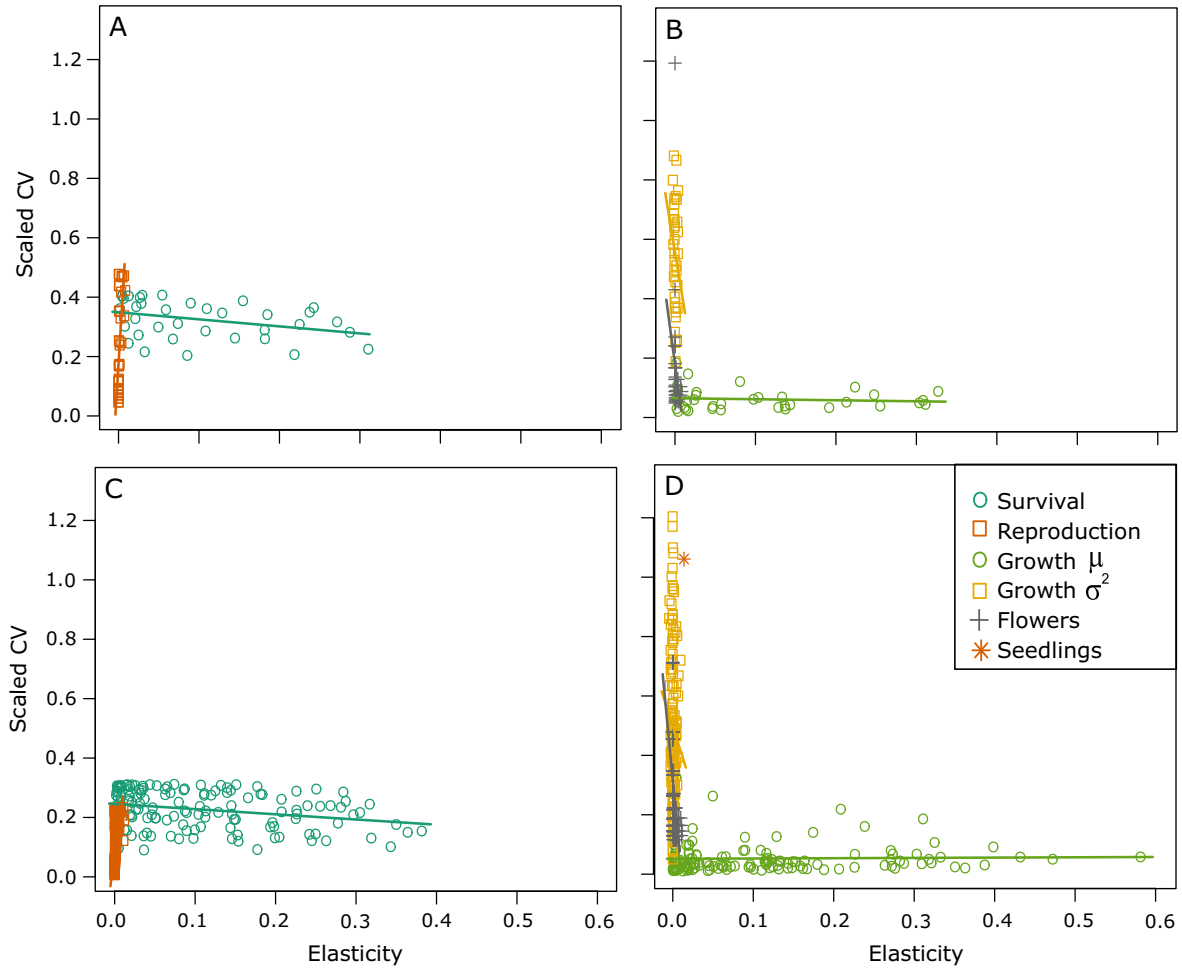

FIG. 5. Relationship between elasticity and variation in vital rates across either (A, B) time or (C, D) space. For rates constrained to lie between 0 and 1, we use relative CV (CV divided by its maximum possible value given a rate's mean value), as a measure of variance, while we use CV for non-constrained rates. Lines show best fit linear regression for values for stage-specific values of each vital rate separately.

TABLE 1. Correlations in vital rate effects across time and space show substantial support for demographic compensation, whereby some vital rates are high under conditions that reduce other rates.

	Survival	Mean growth	Growth variance	Probability reproduction	Flowers	Seedlings/ flower
Survival		**−0.83**	0.19	**−0.80**	0.25	**−0.28**
Mean growth	**−0.066**		**−0.10**	0.77	**−0.36**	0.26
Growth variance	**−0.45**	0.52		0.43	**−0.89**	0.89
Probability reproduction	**−0.50**	0.40	0.19		**−0.78**	0.78
Flowers						**−0.97**

Notes: Top right shows correlation in year effects on each vital rate type, while bottom left shows correlations in transect effects, or spatial correlation in rate variation. Negative correlations shown in boldface type.

than the result of anthropogenic constraints, indicating that one or more mechanisms contribute strongly to its persistence at low numbers. We found partial support for our hypotheses: there was substantial evidence for asynchrony in dynamics as a stabilizing mechanism, but limited evidence that demographic compensation played a strong role in stabilizing the populations (despite operating at some level). Further, our results indicate that negative density dependence is a major factor in explaining the persistence of *Yermo*. Additionally, analyses of both data sets indicate that some areas within the populations may serve as source populations, although whether or not

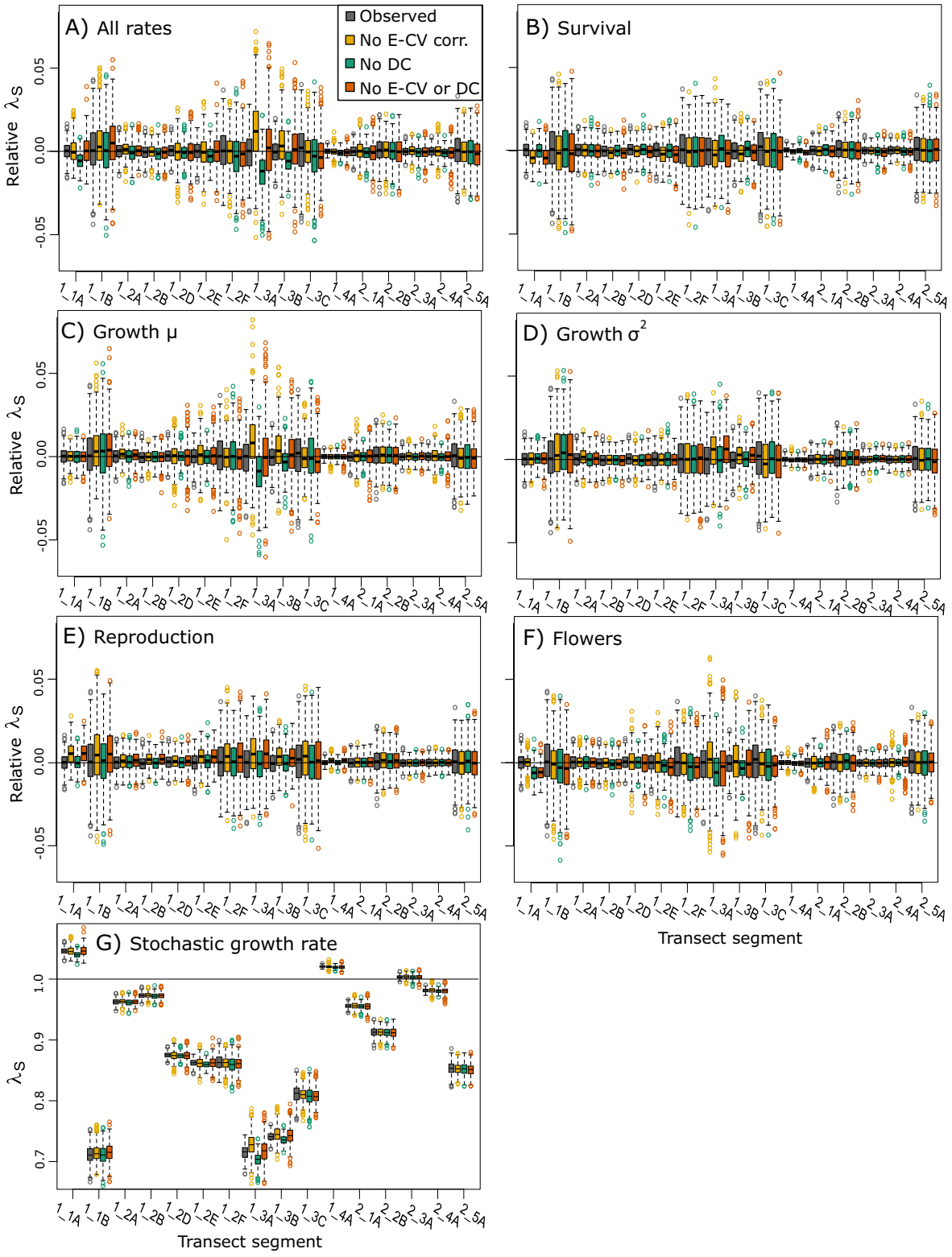

these higher than average growth rates are spatially stable over long periods is unclear. Like demographic compensation, vital rate buffering appears to operate in these populations, but our tests of those effects on population growth rates did not suggest a strong role in stabilizing the populations. We also found support for our second

FIG. 6. Effects of removing elasticity-variation (E-CV) or demographic compensation (DC) patterns on estimated population growth rates. Results come from simulations controlling E-CV, DC or both, and show box plots of growth rates or relative growth, expressed as the difference from that seen in a 100 simulation and the estimated long-term stable λ_s for that population with estimated patterns of variation and correlation (corr.). (A) Relative growth rates with perturbations of DC or E-CV in all vital rates. (B–F) Results for simulations in which only a single vital rate was manipulated to remove observed E-CV or DC patterns. (G) Effects of removing E-CV or DC patterns in all rates, shown for absolute—not relative—population growth rates. Each set of four box plots show stochastic growth rates estimated in 500 simulations of 100 yr each. Each simulation uses the best-fit vital rates models with point estimates of parameter values. Models either used the observed patterns of E-CV and DC, or removed one, the other, or both of these effects. Box plot components are mid line, median; box edges, upper and lower quartiles; whiskers, extending to the upper and lower fences; and points, outliers beyond fences. See Effects of vital rate buffering and demographic rate compensation on population growth for details of randomization approach.

hypothesis, as variation in precipitation had substantial effects in driving spatially asynchronous growth rates across the Sand Draw population.

Negative density dependence can enable populations to recover from low densities through increased population growth and has been shown to stabilize many populations. Its role in the persistence of endemic plant populations could be substantial (Henle et al. 2004, Caughlin et al. 2015), although there are relatively few studies testing for these effects. We found evidence for negative density dependence for the entire Sand Draw population as well as in subpopulations, and this mechanism contributed substantially to long-term population viability in simulations of future numbers. In particular, negative density dependence is an important mechanism allowing subpopulations to recover from unfavorable environmental conditions. Using population models based on more detailed demographic data, which can account for the effects of size structure, we also found some indication of greater population growth rates in lower density transect segments. While negative density dependence could enable establishment in unoccupied areas, we did not see any evidence that *Yermo* expanded its geographic distribution between 1995 and 2013; limited dispersal or, more likely, narrow environmental tolerances could contribute to the restricted and highly stable distribution of the species.

Stability of this population also appears to be augmented by spatial asynchrony in fluctuations among subpopulations and the resulting portfolio effect. In particular, subpopulations became increasingly asynchronous along a north-south axis related to microhabitat variation and in the corresponding interactions with annual precipitation. Most *Yermo* plants in the Sand Draw population occur on or just below steep slopes in the northern portion of population, and density decreases as the landscape flattens toward the south. We found evidence that extremely wet years had a greater negative impact on steeper slopes, perhaps due to the risk of plants being washed out. Conversely, extremely dry years had a more negative effect in flatter areas where neighboring heterospecific plant density is higher, perhaps leading to greater competition for water. Overall, these asynchronous responses to precipitation, as well as additional, unexplained asynchrony in $\log(\lambda)$ across the landscape, strongly reduced the total variability of the Sand Draw population through portfolio effects and contributed to long-term population viability in simulations.

Increasing evidence indicates that portfolio effects are important stabilizing mechanisms in wild populations. Portfolio effects have been especially well studied in fish populations, where asynchrony among populations or distinct habitat types can stabilize total fishery yield (Hilborn et al. 2003, Schindler et al. 2010). Similarly, asynchronous responses of individuals or subpopulations to environmental variation could reduce variability in population growth rates and thus buffer populations from extirpation (Abbott et al. 2017). Asynchrony of the response of different life stages, genotypes, or microhabitats could all generate this effect. For example, disparate responses to environmental variation among life history cohorts in fish (Schindler et al. 2010) or plants (Acker et al. 2014), genotypes or phenotypes within a population (Bolnick et al. 2011), or subpopulations in cryptic microhabitats in plants (Abbott et al. 2017) can all stabilize population numbers. Yet we still have little understanding of the mechanisms underlying these diverse responses to environmental variation. Also, while there has been a surge in interest in the population-stabilizing effects of asynchrony and the portfolio effect (e.g., Moore et al. 2010, Schindler et al. 2015), almost all analyses of these mechanisms to date have been across large spatial scales and multiple populations. The one comparable study on another rare plant (Abbott et al. 2017) showed strong asynchrony effects like those documented here, and also at very fine spatial scales. Together, the results of these studies suggest that such fine-scale portfolio effects may be important in stabilizing dynamics of populations, a previously under-recognized force that may be broadly important in stabilizing populations of rare and restricted species. To date, few studies have tested for fine-scale portfolio effects within small populations; we suggest that designing field sampling so that such tests are possible should be a priority in future work, even for highly restricted species where subtle habitat and climate effects may drive this mechanism.

Both our demographic and census-based analyses showed that some parts of the two *Yermo* populations had significantly more growth than did others. These results could indicate source–sink dynamics at fine scales, with some parts of the populations having reliable net growth and hence subsidizing other population segments. However, even the longer census-based data were not extensive enough to provide a reliable estimate of long-term differences in mean growth rates. Also, the two methods did not

provide concordant predictions of the spatial areas with highest growth rates (Appendix S1: Fig. S19), calling into question whether there are clear source areas.

We also assessed whether demographic compensation or vital rate buffering had substantial effects in increasing population growth rates. While we saw statistical evidence for both patterns, we did not find any strong effect of these mechanisms on population growth rates. Some other studies have found potentially significant effects of demographic rate buffering on extinction risk (Garcia 2003, McDonald et al. 2016), while others have not (Compagnoni et al. 2016). In part, our negative result may be due to the very limited data we have with which to evaluate these effects; with only four annual transitions of data, characterizing the pattern of elasticity vs. variation of vital rates, or the covariance of different rates, is difficult. We also deliberately chose to use a conservative test for vital rate buffering, based on randomization of variances only within vital rates, rather than across rates. Past work on vital rate buffering has generally randomized across all rates and stages (Pfister 1998, Morris and Doak 2004) to assess the power of this pattern. At least for our study species, however, the quite different ranges of relative variation for different rates made this approach seem too unrealistic. While we did not find support for these two mechanisms in strongly increasing mean growth rates, these effects could be better supported with more extensive data. However, recent surveys have tended to show only weak patterns of buffering, in particular, suggesting that it may be of limited strength for many species (Jongejans et al. 2010, Jakalaniemi et al. 2013, Bjørkvoll et al. 2016, McDonald et al. 2016).

One further mechanism that may confer resiliency to small populations is metapopulation dynamics, where individuals can migrate among populations to stabilize numbers or recolonize extirpated habitat areas. While this mechanism has been the subject of considerable conservation interest, it is unlikely to have any importance for *Yermo*. Because this species naturally occurs in only two small, isolated populations, this type of rescue and recolonization is unlikely to have a role in stabilizing populations or reducing extinction risk.

Our findings also highlight the contrasting strengths of intensive, relatively short-term demographic studies vs. longer-term count-based approaches to characterizing population dynamics (Morris and Doak 2002). While researchers often do not have the luxury to choose between these approaches, we were able to compare insights from both types of data. We found that longer term census data gave more realistic, higher estimates of population stability than did our shorter-term demographic study. In part, this difference comes from the fairly dry conditions that prevailed during the years of our demographic data collection, which suppressed *Yermo* performance and hence estimated growth rates. Beyond this difference, the long-term census data provided clear evidence of weak but critical density dependence that boosts population growth at lower densities, as well as clear asynchrony in local dynamics. These two effects strongly stabilize the population, and evidence for them had to come from relatively long-term data. While, in our case, census data were clearly more powerful in assessing stability mechanisms, the strength of the data set came from its careful and detailed collection. In particular, unlike most count data used in PVAs, these were complete, spatially structured censuses of the main population of *Yermo*; Richard and Beverly Scott, who collected these data, made every effort to count all individuals in a consistent manner over many years. Furthermore, the consistent, careful spatial indexing of these counts was critical in allowing estimation of fine-scale portfolio effects. We are aware of very few count-based studies that have these features, which were crucial to our analyses.

Overall, *Yermo* appears to rely on several stabilizing mechanisms that operate at fine spatial scales. This study supports a role for variation in microhabitats to generate stable populations, even for highly restricted species. Other studies have found a diversity of responses to environmental conditions among subpopulations of restricted plants (Fréville et al. 2004, Maliakal-Witt et al. 2004, Severns 2008), but rarely have these differences been analyzed for their effects on population stability (but see Crone 2016). One caveat to our main result of population stability is that these predictions depend on assumptions about future climate variation. What remains unclear is whether or not Central Wyoming will face wetter or drier conditions with climate change (Shinker and Bartlein 2010), or how increasing temperatures will mediate effects of moisture for *Yermo*. Thus, as with most other species, we still lack the ability to predict confidently the dynamics with changing abiotic conditions.

Acknowledgments

Richard and Beverly Scott and their teams of volunteers established the population survey of the main *Yermo* site and maintained this extraordinary and exacting data collection effort for a decade. The analyses we report here would not have been possible without their efforts, or their willingness to share their data and consult on their methods. Many volunteers and field assistants also provided invaluable assistance in the data collection for both the demographic and census sampling. Both Bonnie Heidel and Tyler Abbott provided assistance and information that aided in the initiation and completion of this work. The Bureau of Land Management provided funding supporting much of the fieldwork for this study. Additional funding supporting data analyses was supplied by NSF awards 1340024 and 1242355 and a LABEX/Tulip visiting scientist travel award to D. F. Doak.

Literature Cited

Abbott, R. E., D. F. Doak, and M. L. Peterson. 2017. Portfolio effects, climate change, and the persistence of small populations: analyses on the rare plant *Saussurea weberi*. Ecology 98:1071–1081.

Acker, P., A. Robert, R. Bourget, and B. Colas. 2014. Heterogeneity of reproductive age increases the viability of semelparous populations. Functional Ecology 28:458–468.

Anderson, S. C., A. B. Cooper, and N. K. Dulvy. 2013. Ecological prophets: quantifying metapopulation portfolio effects. Methods in Ecology and Evolution 4:971–981.

Bakker, V. J., D. F. Doak, G. W. Roemer, D. K. Garcelon, T. J. Coonan, S. A. Morrison, C. Lynch, K. Ralls, and R. Shaw. 2009. Incorporating ecological drivers and uncertainty into a demographic population viability analysis for the island fox. Ecological Monographs 79:77–108.

Barot, S., and J. Gignoux. 2004. How do sessile dioecious species cope with their males? Theoretical Population Biology 66:163–173.

Bates, D., M. Mächler, B. Bolker, and S. Walker. 2015. Fitting linear mixed-effects models using lme4. Journal of Statistical Software 67:1–48.

Bjørkvoll, E., A. M. Lee, V. Grøtan, B. Sæther, A. Stien, S. Engen, S. Albon, and B. B. Hansen. 2016. Demographic buffering of life histories? Implications of the choice of measurement scale. Ecology 97:40–47.

Bolnick, D. I., P. Amarasekare, M. S. Araújo, R. Bürger, J. M. Levine, M. Novak, V. H. Rudolf, S. J. Schreiber, M. C. Urban, and D. A. Vasseur. 2011. Why intraspecific trait variation matters in community ecology. Trends in Ecology & Evolution 26:183–192.

Boyce, M. S., et al. 2006. Demography in an increasingly variable world. Trends in Ecology & Evolution 21:141–148.

Brown, L. M., and E. E. Crone. 2016. Individual variation changes dispersal distance and area requirements of a checkerspot butterfly. Ecology 97:106–115.

Caswell, H. 2001. Matrix population models: construction, analysis, and interpretation. Second edition. Sinauer Associates, Sunderland, Massachusetts, USA.

Caughlin, T. T., J. M. Ferguson, J. W. Lichstein, P. A. Zuidema, S. Bunyavejchewin, and D. J. Levey. 2015. Loss of animal seed dispersal increases extinction risk in a tropical tree species due to pervasive negative density dependence across life stages. Proceedings of the Royal Society B 282:20142095.

Compagnoni, A., et al. 2016. The effect of demographic correlations on the stochastic population dynamics of perennial plants. Ecological Monographs 86:125–144.

Crone, E. 2016. Contrasting effects of spatial heterogeneity and environmental stochasticity on population dynamics of a perennial wildflower. Journal of Ecology 104:281–291.

Dennis, B., P. L. Munholland, and J. M. Scott. 1991. Estimation of growth and extinction parameters for endangered species. Ecological Monographs 61:115–143.

Dias, P. C. 1996. Sources and sinks in population biology. Trends in Ecology & Evolution 11:326–330.

Dirnböck, T., F. Essl, and W. Rabitsch. 2011. Disproportional risk for habitat loss of high-altitude endemic species under climate change: habitat loss of high-altitude endemics. Global Change Biology 17:990–996.

Doak, D. F. 1995. Source–sink models and the problem of habitat degradation: general models and applications to the Yellowstone Grizzly. Conservation Biology 9:1370–1379.

Doak, D. F., and W. F. Morris. 2010. Demographic compensation and tipping points in climate-induced range shifts. Nature 467:959–962.

Doak, D. F., D. Bigger, E. K. Harding, M. A. Marvier, R. E. O'Malley, and D. Thomson. 1998. The statistical inevitability of stability-diversity relationships in community ecology. American Naturalist 151:264–276.

Easterling, M. R., S. P. Ellner, and P. M. Dixon. 2000. Size-specific sensitivity: applying a new structured population model. Ecology 81:694–704.

Ellner, S. P., and M. Rees. 2006. Integral projection models for species with complex demography. American Naturalist 167:410–428.

Fiedler, P. L. 1987. Life history and population dynamics of rare and common mariposa lilies (Calochortus Pursh: Liliaceae). Journal of Ecology 75:977–995.

Fisher, R. A., A. S. Corbet, and C. B. Williams. 1943. The relation between the number of species and the number of individuals in a random sample of an animal population. Journal of Animal Ecology 12:42–58.

Fréville, H., B. Colas, M. Riba, H. Caswell, A. Mignot, E. Imbert, and I. Olivieri. 2004. Spatial and temporal demographic variability in the endemic plant species *Centaurea corymbosa* (Asteraceae). Ecology 85:694–703.

Garcia, M. B. 2003. Demographic viability of a relict population of the critical endangered plant *Borderea choudardii*. Conversation Biology 17:1672–1680.

Gaston, K. J., and W. E. Kunin. 1997. Rare—common differences: an overview. Pages 12–29 *in* W. E. Kunin and K. J. Gaston, editors. The biology of rarity. Springer, Dordrecht, The Netherlands.

Ginzburg, L. R., S. Ferson, and H. R. Akçakaya. 1990. Reconstructibility of density dependence and the conservative assessment of extinction risks. Conservation Biology 4:63–70.

Heidel, B., J. Handley, and M. Andersen. 2011. Distribution and habitat requirements of *Yermo xanthocephalus* (Desert yellowhead), Fremont County, Wyoming. Report prepared for the USDI Bureau of Land Management, Wyoming State Office by the Wyoming Natural Diversity Database, University of Wyoming, Laramie, Wyoming, USA.

Henle, K., S. Sarre, and K. Wiegand. 2004. The role of density regulation in extinction processes and population viability analysis. Biodiversity and Conservation 13:9–52.

Hilborn, R., T. P. Quinn, D. E. Schindler, and D. E. Rogers. 2003. Biocomplexity and fisheries sustainability. Proceedings of the National Academy of Sciences USA 100:6564–6568.

Honnay, O., and H. Jacquemyn. 2007. Susceptibility of common and rare plant species to the genetic consequences of habitat fragmentation. Conservation Biology 21:823–831.

Jakalaniemi, A., S. Ramula, and J. Tuomi. 2013. Variability of important vital rates challenges the demographic buffering hypothesis. Evolutionary Ecology 27:533–545.

Jongejans, E., H. de Kroon, S. Tuljapurkar, and K. Shea. 2010. Plant populations track rather than buffer climate fluctuations. Ecology Letters 13:736–743.

Kauffman, M. J., J. F. Pollock, and B. Walton. 2004. Spatial structure, dispersal, and management of a recovering raptor population. American Naturalist 164:582–597.

Lloret, F., A. Escudero, J. M. Iriondo, J. Martínez-Vilalta, and F. Valladares. 2012. Extreme climatic events and vegetation: the role of stabilizing processes. Global Change Biology 18:797–805.

Loreau, M., and C. de Mazancourt. 2008. Species synchrony and its drivers: neutral and nonneutral community dynamics in fluctuating environments. American Naturalist 172:E48–E66.

Maliakal-Witt, S., E. S. Menges, and J. S. Denslow. 2004. Microhabitat distribution of two Florida scrub endemic plants in comparison to their habitat-generalist congeners. American Journal of Botany 92:411–421.

Maschinski, J., J. E. Baggs, P. F. Quintana-Ascencio, and E. S. Menges. 2006. Using population viability analysis to predict the effects of climate change on the extinction risk of an endangered limestone endemic shrub, Arizona cliffrose: rare plant extinction risk with climate change. Conservation Biology 20:218–228.

McDonald, J. L., T. Bailey, R. J. Delahay, R. A. McDonald, G. C. Smith, and D. J. Hodgson. 2016. Demographic buffering and compensatory recruitment promotes the persistence of disease in a wildlife population. Ecology Letters 19:443–449.

Moore, J. W., M. McClure, L. A. Rogers, and D. E. Schindler. 2010. Synchronization and portfolio performance of threatened salmon. Conservation Letters 3:340–348.

Morris, W. F., and D. F. Doak. 2002. Quantitative conservation biology: theory and practice of population viability analysis. Sinauer Associates, Sunderland, Massachusetts, USA.

Morris, W. F., and D. F. Doak. 2004. Buffering of life histories against environmental stochasticity: accounting for a spurious correlation between the variabilities of vital rates and their contributions to fitness. American Naturalist 163:579–590.

Palmer, T. M., D. F. Doak, M. L. Stanton, J. L. Bronstein, E. T. Kiers, T. P. Young, J. R. Goheen, and R. M. Pringle. 2010. Synergy of multiple partners, including freeloaders, increases host fitness in a multispecies mutualism. Proceedings of the National Academy of Sciences USA 107:17234–17239.

Pfister, C. A. 1998. Patterns of variance in stage-structured populations: evolutionary predictions and ecological implications. Proceedings of the National Academy of Sciences USA 95:213–218.

Preston, F. W. 1948. The commonness, and rarity, of species. Ecology 29:254–283.

Pulliam, H. R. 1988. Sources, sinks, and population regulation. American Naturalist 132:652–661.

R Core Team. 2016. R: A language and environment for statistical computing. R Foundation for Statistical Computing, Vienna, Austria. https://www.R-project.org/

Rabinowitz, D. 1981. Seven forms of rarity. Pages 205–217 *in* H. Synge, editor. The biological aspects of rare plants conservation. Wiley, Chichester, UK.

Rabinowitz, D., S. Cairns, and T. Dillon. 1986. Seven forms of rarity and their frequency in the flora of the British Isles. Pages 182–204 *in* M. E. Soule, editor. Conservation biology, the science of scarcity and diversity. Sinauer, Sunderland, Massachusetts, USA.

Raventós, J., E. González, E. Mújica, and D. F. Doak. 2015. Population viability analysis of the epiphytic ghost orchid (*Dendrophylax lindenii*) in Cuba. Biotropica 47:179–189.

Ricker, W. E. 1954. Stock and recruitment. Journal of the Fisheries Research Board of Canada 11:559–623.

Rotella, J. J., W. A. Link, T. Chambert, G. E. Stauffer, and R. A. Garrot. 2011. Evaluating the demographic buffering hypothesis with vital rates estimated for Weddell seals from 30 years of mark-recapture data. Journal of Animal Ecology 81:162–173.

Schindler, D. E., R. Hilborn, B. Chasco, C. P. Boatright, T. P. Quinn, L. A. Rogers, and M. S. Webster. 2010. Population diversity and the portfolio effect in an exploited species. Nature 465:609–612.

Schindler, D. E., J. B. Armstrong, and T. E. Reed. 2015. The portfolio concept in ecology and evolution. Frontiers in Ecology and the Environment 13:257–263.

Scott, R. W., and B. J. Scott. 2009. *Yermo xanthocephalus* Dorn: a research report. Prepared for Bureau of Land Management. Central Wyoming College Herbarium and Scott Environmental Resources, Inc. in cooperation with Wyoming Natural Diversity Database. Riverton, WY.

Severns, P. M. 2008. Seedling population size and microhabitat association in *Lupinus oreganos* A. Heller var. *kincaidii* C.P. Sm. (Fabaceae) a threated plant of western Oregon grasslands. Native Plants Journal 9:358–365.

Shinker, J. J., and P. J. Bartlein. 2010. Spatial variations of effective moisture in the western United States. Geophysical Research Letters 37:L02701.

Sinclair, A. R. E., and R. P. Pech. 1996. Density dependence, stochasticity, compensation and predator regulation. Oikos 75:164–173.

Thibaut, L. M., and S. R. Connolly. 2013. Understanding diversity-stability relationships: towards a unified model of portfolio effects. Ecology Letters 16:140–150.

USDI Fish and Wildlife Service. 2002. Endangered and threatened wildlife and plants: Listing the desert yellowhead as threatened. Federal Register 50:11442–11449.

Villellas, J., D. F. Doak, M. B. García, and W. F. Morris. 2015. Demographic compensation among populations: what is it, how does it arise and what are its implications? Ecology Letters 18:1139–1152.

Yenni, G., P. B. Adler, and S. K. Ernest. 2012. Strong self-limitation promotes the persistence of rare species. Ecology 93:456–461.

Supporting Information

Additional supporting information may be found online at: http://onlinelibrary.wiley.com/doi/10.1002/ecm.1360/full

Data Availability

Data are available from the Dryad Digital Repository: https://doi.org/10.5061/dryad.3ps1513.